

# New Spin-Wave Propagation Length Scales in Low Damping Metallic Ferromagnets

Luis Flacke,<sup>1,2, a)</sup> Lukas Liensberger,<sup>1,2</sup> Matthias Althammer,<sup>1,2</sup> Hans Huebl,<sup>1,2,3,4</sup> Stephan Geprgs,<sup>1</sup> Katrin Schultheiss,<sup>5</sup> Aleksandr Buzdakov,<sup>5</sup> Tobias Hula,<sup>5</sup> Helmut Schultheiss,<sup>5</sup> Eric R. J. Edwards,<sup>6</sup> Hans T. Nembach,<sup>6</sup> Justin M. Shaw,<sup>6</sup> Rudolf Gross,<sup>1,2,3,4</sup> and Mathias Weiler<sup>1,2, b)</sup>

<sup>1)</sup> *Walther-Meiner Institute, Bayerische Akademie der Wissenschaften, 85748 Garching, Germany*

<sup>2)</sup> *Physics Department, Technical University of Munich, 85748 Garching, Germany*

<sup>3)</sup> *Nanosystems Initiative Munich, 80799 Munich, Germany*

<sup>4)</sup> *Munich Center for Quantum Science and Technology (MCQST), 80799 Munich, Germany*

<sup>5)</sup> *Helmholtz-Zentrum Dresden-Rossendorf, 01328 Dresden, Germany*

<sup>6)</sup> *Quantum Electromagnetics Division, National Institute of Standards and Technology, Boulder, CO 80305, USA*

We report ultra-low intrinsic magnetic damping in  $\text{Co}_{25}\text{Fe}_{75}$  heterostructures, reaching the low  $10^{-4}$  regime at room temperature. By using a broadband ferromagnetic resonance technique, we extracted the dynamic magnetic properties of several  $\text{Co}_{25}\text{Fe}_{75}$ -based heterostructures with varying ferromagnetic layer thickness. By estimating the eddy current contribution to damping, measuring radiative damping and spin pumping effects, we extrapolated an intrinsic damping of  $\alpha_0 \leq 3.05 \times 10^{-4}$ . Furthermore, using Brillouin light scattering microscopy we measured spin-wave propagation lengths of up to  $(21 \pm 1) \mu\text{m}$  in a 26 nm thick  $\text{Co}_{25}\text{Fe}_{75}$  heterostructure at room temperature, which is in excellent agreement with the measured damping.

Itinerant ferromagnets (FM) are advantageous for spintronic and magnonic devices. They benefit from, e.g., large magnetoresistive effects and current-induced spin-orbit torques<sup>1</sup>. In many magneto-resistive technologies (e.g., anisotropic magnetoresistance, giant magnetoresistance, tunnel magnetoresistance) electronic conductivity is indispensable. Moreover, due to high saturation magnetization in metallic FMs, spin-wave group velocities are in general significantly higher than in insulating ferrimagnets<sup>2-5</sup>. High saturation magnetizations in general ease detection. Nevertheless, itinerant FMs typically have considerable magnetic damping<sup>6,7</sup>. This is unfavorable for many applications. For example, low damping is crucial for oscillators based on spin transfer torques and spin orbit torques as well as for achieving large spin-wave propagation lengths<sup>8-10</sup>. The need for thin film materials with low magnetic damping has triggered the interest in the insulating ferrimagnet yttrium-iron garnet ( $\text{Y}_3\text{Fe}_5\text{O}_{12}$ , YIG)<sup>11-13</sup>. Although for YIG, very small total (Gilbert) damping parameters in the order of  $\alpha_G \approx 10^{-5}$ , and large spin-wave propagation lengths of a few tens of micrometers (up to  $\sim 25 \mu\text{m}$ ) in thin films ( $\sim 20 \text{nm}$ ) have been reported<sup>5,13,14</sup>, it has low electrical conductivity.

Schoen *et al.* recently observed ultra-low intrinsic magnetic damping in  $\text{Co}_{25}\text{Fe}_{75}$  (simply referred to as CoFe in the following) metallic thin films ( $\alpha_0 = (5 \pm 1.8) \times 10^{-4}$ )<sup>15</sup>, and Krner *et al.* reported propagation lengths of  $5 \mu\text{m} - 8 \mu\text{m}$  in CoFe using time resolved scanning magneto-optical Kerr microscopy<sup>4</sup>. This motivated our study on sputter-deposited CoFe-based thin film heterostructures. We use broadband ferromagnetic resonance (BB-FMR) spectroscopy<sup>16</sup> and Brillouin light scattering

(BLS) microscopy<sup>17</sup> and find intrinsic damping parameters in the low  $10^{-4}$  regime as well as spin-wave propagation lengths of more than  $20 \mu\text{m}$ . The damping is thus comparable to YIG/heavy metal (HM) heterostructures<sup>18</sup> and the spin-wave propagation length is comparable to that of state-of-the-art YIG thin films<sup>5,13</sup>. Thus,  $\text{Co}_{25}\text{Fe}_{75}$  combines low magnetic damping with good electrical conductivity and large saturation magnetization, making it a promising material for all-metal magnonic devices.

For BB-FMR,  $\text{Ta}(3 \text{nm})/\text{Al}(3 \text{nm})/\text{Co}_{25}\text{Fe}_{75}(t)/\text{Al}(3 \text{nm})/\text{Ta}(3 \text{nm})$  heterostructures with different thickness  $t$  of the CoFe layer were sputter deposited on a thermally oxidized Si (100) substrate at an Ar pressure of  $5 \times 10^{-6}$  bar at room temperature. No subsequent annealing process was performed. The CoFe layer thickness was varied between  $1.4 \text{nm} < t < 26 \text{nm}$  as determined by X-ray reflectometry.

The out of plane BB-FMR measurements were performed at room temperature with a vector network analyzer (VNA). The samples were placed directly on a coplanar waveguide (CPW), with a  $80 \mu\text{m}$  wide center conductor. For the measurements, the VNA frequency  $f$  was kept constant and the microwave transmission parameter  $S_{21}$  was recorded as a function of applied magnetic field  $H_0$  for a range of frequencies at an VNA output power of 0 dBm. A representative set of data as measured of the real and imaginary part of  $S_{21}$  at 16 GHz for samples with  $t = 1.8 \text{nm}$  and  $t = 26 \text{nm}$  is shown in Fig. 1 (a) and (b). We fit the raw data with

$$S_{21}(H_0) = S_{21}^0 + iA \frac{\chi(H_0)}{M_s} = S_{21}^0 (1 + \Delta S_{21}), \quad (1)$$

where

$$\chi(H_0) = \frac{M_s(H_0 - H_{\text{res}} + H_{\text{eff}} + i\Delta H)}{(H_0 - H_{\text{res}} + H_{\text{eff}} + i\Delta H)^2 - H_{\text{eff}}^2} \quad (2)$$

<sup>a)</sup> Electronic mail: luis.flacke@wmi.badw.de

<sup>b)</sup> Electronic mail: mathias.weiler@wmi.badw.de

is the magnetic response of the FM, which is obtained by solving the Landau-Lifshitz-Gilbert equation (LLG). Here,  $S_{21}^0$  is the background transmission through the CPW without magnetic resonance peak. It is determined from the fits as a complex linear background to the data  $S_{21}^0(H_0) = S_{21}^a + H_0 S_{21}^b$ . The factor  $A$  is a complex-valued scaling parameter,  $M_s$  is the saturation magnetization of the sample,  $H_{\text{res}}$  is the resonance field,  $H_{\text{eff}} = 2\pi f / (\mu_0 \gamma)$ , with  $\gamma = g\mu_B/\hbar$ , where  $g$  is the Land factor,  $\mu_B$  is the Bohr magneton,  $\hbar$  is the reduced Planck constant and  $\Delta H$  is the full width at half maximum (FWHM) linewidth of the resonance. A detailed derivation of the susceptibility can be found in Ref. 19.

In the out-of-plane (OOP) geometry, the resonance condition for thin films is given by<sup>20</sup>

$$\mu_0 H_{\text{res}} = \mu_0 M_{\text{eff}} + \mu_0 H_{\text{eff}}, \quad (3)$$

where  $M_{\text{eff}} = M_s - H_k$  is the effective magnetization, with the uniaxial out-of-plane anisotropy field  $H_k$ . In Fig. 1 (c), we plot the determined  $H_{\text{res}}$  vs. the frequency  $f$ . From the fit to Eq. (3) (red solid lines in Fig. 1 (c)), we obtain  $M_{\text{eff}}$  and the Land-factor  $g$  of the specific sample.

The FWHM linewidth vs. frequency data shown in Fig. 1 (d) is fitted to

$$\mu_0 \Delta H = \mu_0 H_{\text{inh}} + 2 \cdot \frac{2\pi f \alpha_G}{\gamma}. \quad (4)$$

Here,  $H_{\text{inh}}$  is the inhomogeneous linewidth broadening and  $\alpha_G$  is the phenomenological Gilbert damping parameter<sup>21,22</sup>.

Several contributions to the measured total damping ( $\alpha_G$ ) were extracted from our data. In addition to the intrinsic damping of the magnetic material itself ( $\alpha_0$ ), spin pumping ( $\alpha_{\text{sp}}$ ) contributes significantly<sup>23,24</sup> to the total damping in our thinner heterostructures due to the adjacent HM (Ta) layers<sup>25</sup>. Furthermore, we consider additional damping contributions from eddy currents ( $\alpha_{\text{eddy}}$ ) and radiative damping ( $\alpha_{\text{rad}}$ )<sup>15,19</sup>. Due to these contributions, the total damping ( $\alpha_G = \alpha_0 + \alpha_{\text{sp}} + \alpha_{\text{eddy}} + \alpha_{\text{rad}}$ ) depends on the FM thickness. We calculated damping due to eddy currents and measured radiative damping contributions to the total damping. The eddy current contribution is given by<sup>15</sup>  $\alpha_{\text{eddy}} = \gamma \mu_0^2 M_s t^2 / 16\rho$ , with  $\mu_0 M_s$  and resistivity  $\rho$  of the CoFe thin film. The saturation magnetization  $\mu_0 M_s = 2.36$  T is given by the  $y$ -intercept of a linear fit to  $M_{\text{eff}}$  vs.  $1/t$  (see Fig. 2 (a)) and the resistivity  $\rho = 340$  n $\Omega$  m is a weighted averaged value from iron and cobalt thin film resistivities with film thicknesses of around 20 nm<sup>26,27</sup>. From this simplistic analysis we find an almost negligible eddy current contribution to the total damping  $\alpha_G$  of < 5%. A quantitative determination analogous to Ref. 19 of the radiative damping is done by analyzing the magnitude of the measured inductance  $L$  of all samples. With Eq. (1) above and Eq. (9) from Ref. 19, one obtains:

$$\frac{L}{\chi} \equiv \tilde{L} = -\frac{2Z_0 A}{\mu_0 M_s S_{21}^0 \omega}. \quad (5)$$

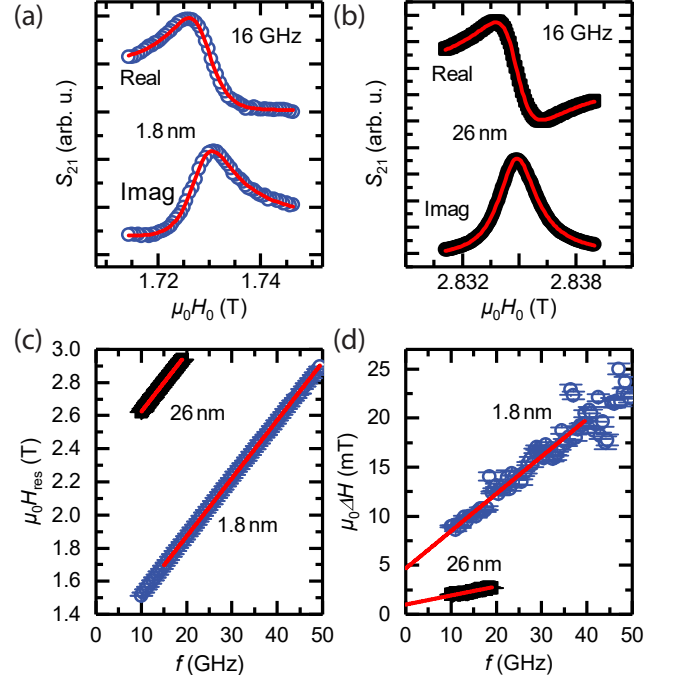


FIG. 1. (a), (b) Measured microwave transmission  $S_{21}$  at 16 GHz plotted vs. applied magnetic field  $H_0$  for blanket Ta(3 nm)/Al(3 nm)/Co<sub>25</sub>Fe<sub>75</sub>( $t$ )/Al(3 nm)/Ta(3 nm) samples with CoFe thickness  $t = 1.8$  nm ((a) blue symbols) and  $t = 26$  nm ((b) black symbols), respectively. The red lines are fits of Eq. (1) to the data. The extracted resonance fields  $H_{\text{res}}$  and linewidths  $\Delta H$  as a function of the applied microwave frequency are shown in (c) and (d), respectively. Here, the error bars (smaller than symbol size) are extracted fit errors from (a) and (b). In (c) the red line is a fit to Eq. (3) to extract the Land-factor  $g$  and the effective magnetization  $M_{\text{eff}}$ . In (d), the linewidth is plotted vs. frequency. The Gilbert parameter  $\alpha_G$  and the inhomogeneous linewidth broadening  $H_{\text{inh}}$  are extracted by fitting the data to Eq. (4) (red lines).

Here,  $Z_0 = 50 \Omega$  is the CPW impedance. It has been shown, that  $\tilde{L} = \tilde{L}_0 + \tilde{L}_1(\omega)$ , where  $\tilde{L}_0 \in \mathbb{R}$  and  $\tilde{L}_1 \in \mathbb{C}$ , due to the effect of inverse spin-orbit torques<sup>19</sup>. We extract  $L$  from the FMR measurements, and the dipolar inductance  $\tilde{L}_0$  from a fit of  $\tilde{L}$  vs.  $f$  for each sample. The radiative damping contribution is then given as<sup>19</sup>

$$\alpha_{\text{rad}} = \frac{1}{4} \frac{\gamma \mu_0 M_s}{Z_0} \tilde{L}_0. \quad (6)$$

This analysis allows us to determine  $\alpha_{\text{rad}}$  independently of geometrical parameters of the samples or CPWs and is used to quantitatively extract the dipolar inductance without any calibration of the microwave circuit. For the thickest sample we obtain  $\alpha_{\text{rad}} = (4.69 \pm 0.05) \times 10^{-4}$ , which is comparable to previously obtained values<sup>15,28</sup>. The spin pumping contribution  $\alpha_{\text{sp}}$  is given by

$$\alpha_{\text{sp}} = 2 \frac{\gamma \hbar g_{\text{eff}}^{\uparrow\downarrow}}{4\pi M_s t}, \quad (7)$$

where  $g_{\text{eff}}^{\uparrow\downarrow}$  is the effective spin mixing conductance<sup>15</sup>. We

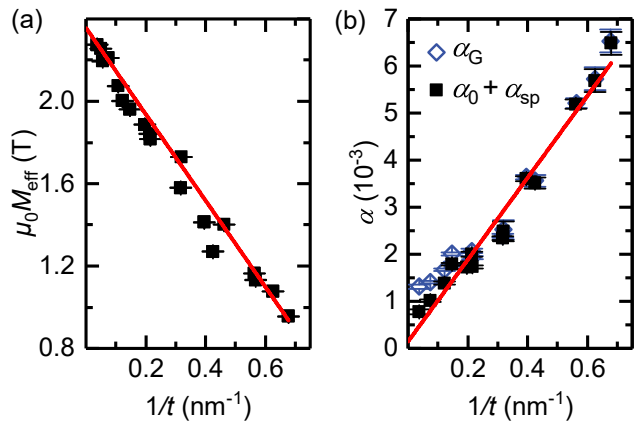


FIG. 2. (a) The effective magnetization is extracted using Eq. (3) for each sample and is plotted vs. the reciprocal FM thickness. From a linear fit (red line), the saturation magnetization  $\mu_0 M_s = (2.36 \pm 0.02)$  T is determined as the extrapolated bulk value, assuming vanishing volume anisotropy<sup>30</sup>. In (b) the total Gilbert damping (blue diamonds) and the spin pumping behavior together with the intrinsic damping (black squares) are shown. The error bars depicted in both panels are fit errors. For thicker samples the available frequency range is rather small (see Fig. 1(d)), the limited frequency range leads to an additional uncertainty, as discussed in Ref. 31. The red line is an unweighted fit to Eq. (7).

subtract  $\alpha_{\text{rad}}$  and  $\alpha_{\text{eddy}}$  from the measured total damping  $\alpha_G$  and plot the remaining damping  $\alpha_0 + \alpha_{\text{sp}}$  as a function of  $1/t$  in Fig. 2(b) together with the total damping  $\alpha_G$ . From a linear fit (Eq. (7)) to  $\alpha_0 + \alpha_{\text{sp}}$ , we obtain the intrinsic damping  $\alpha_0 = (1.45 \pm 1.60) \times 10^{-4}$  from the  $y$ -intercept. This is the lowest measured intrinsic damping of a ferromagnetic metal so far. For the fit, we use  $\mu_0 M_s$  as above and  $\gamma/2\pi = 28.55$  GHz/T. The fitted effective spin mixing conductance  $g_{\text{eff}} = (5.3 \pm 0.3) \times 10^{18} \text{ m}^{-2}$  is in agreement with literature values<sup>15</sup>. We attribute the slightly reduced intrinsic  $\alpha_0$  compared to Ref. 28 to the use of a different seed layer, which has a substantial impact on the damping of CoFe<sup>29</sup>.

The low damping properties of the CoFe heterostructures, in combination with the high saturation magnetization are expected to result in long propagation lengths of dipolar spin waves. We use microfocused BLS<sup>17</sup> to study the spin-wave propagation in patterned CoFe samples, which are schematically depicted in Fig. 3(a) and (b).

For our experiments, we fabricated patterned stripes of a Pt(3 nm)/Cu(3 nm)/Co<sub>25</sub>Fe<sub>75</sub>( $t$ )/Cu(3 nm)/Ta(3 nm) heterostructure using laser (sample A) and electron beam (sample B) lithography, sputter deposition and a subsequent lift-off process. This stack sequence was used as lower in plane damping was observed compared to the samples containing Al. Below, we present data on only two samples with a thickness of  $t = 5$  nm and a width  $w = 1.5 \mu\text{m}$  for sample A and  $t = 26$  nm and  $w = 5 \mu\text{m}$  for sample B, respectively. An aluminum antenna was

placed on top of the CoFe strip to drive spin dynamics via a microwave drive applied to the antenna. For sample A we used a simple aluminum strip, whereas for the sample B we used a CPW antenna optimized for an efficient excitation of spin waves with wave number  $k \approx 1 \mu\text{m}^{-1}$ . The driving power was chosen to be in the linear excitation regime.

In order to compare the linewidths of extended and patterned films, we used sample A in backward volume geometry and placed the laser spot close to the antenna. We recorded BLS spectra for several magnetic fields for each frequency. The BLS intensity is integrated and the signal sum is then plotted vs. the external magnetic field in Fig. 3(c). The FWHM-linewidth  $\Delta H$  is determined by fitting a Lorentzian (red line). We then compared the fitted linewidth to that of a blanket film, deposited simultaneously with the structured BLS sample, and measured with in-plane BB-FMR. In the in-plane configuration the total damping increases due to magnon-magnon scattering<sup>32</sup>. As shown in Fig. 3(d), the linewidths  $\mu_0 \Delta H$  determined from BB-FMR (black symbols) and BLS (blue symbols) are very similar, indicating that the damping properties are not affected by the patterning, as expected in a lift-off process with micrometer feature sizes.

In the next set of experiments, we investigate the spin-wave propagation length of sample B (see Fig. 3(b)). Here, the magnitude of the external magnetic field was fixed at  $\mu_0 H_0 = 43$  mT, while the field was applied perpendicular to the CoFe strip (Damon-Eshbach geometry). The BLS intensity was recorded as a function of position ( $x, y$ ) over the CoFe strip. The BLS intensity decay in  $x$  direction (i.e. the BLS intensity averaged over the width of the strip in order to suppress mode-beating effects<sup>33-35</sup>) is shown in Fig. 3(e) for  $f = 9.5$  GHz. The propagation length  $\lambda_{\text{prop}}$  is extracted by a fit to  $I = I_0 \exp(-2x/\lambda_{\text{prop}})$ <sup>36</sup> and plotted vs.  $f$  in Fig. 3(f). The factor of two in the exponent comes from the quadratic relation between spin-wave intensity and amplitude. From our experiments, we extract a maximum propagation length of  $(21 \pm 1) \mu\text{m}$ , well exceeding previously obtained results for FeNi alloys<sup>37</sup> and CoFe<sup>4</sup> and very comparable to values found for YIG thin films<sup>5,13</sup>. The red curve is the theoretical prediction, based on the analytical Kalinikos-Slavin model detailed below and using the magnetic parameters determined by in-plane BB-FMR ( $\mu_0 M_s = 2.36$  T,  $\alpha_G - \alpha_{\text{rad}} = 3.90 \times 10^{-3}$ ,  $g = 2.061$ ) for a co-deposited reference sample.

Starting with Kalinikos and Slavin's spin-wave dispersion for the modes with  $\mathbf{k}_x \perp \mathbf{M}^{38}$

$$f_{\text{res}} = \frac{\mu_0 \gamma}{2\pi} \sqrt{H_0 + H_d + H_k + M_s \frac{1 - \exp(-kt)}{kt}} \times \sqrt{H_0 + H_d + M_s \left(1 - \frac{1 - \exp(-kt)}{kt}\right)}, \quad (8)$$

we calculated the group velocity  $v_g = 2\pi \partial f_{\text{res}} / \partial k$ . Here,

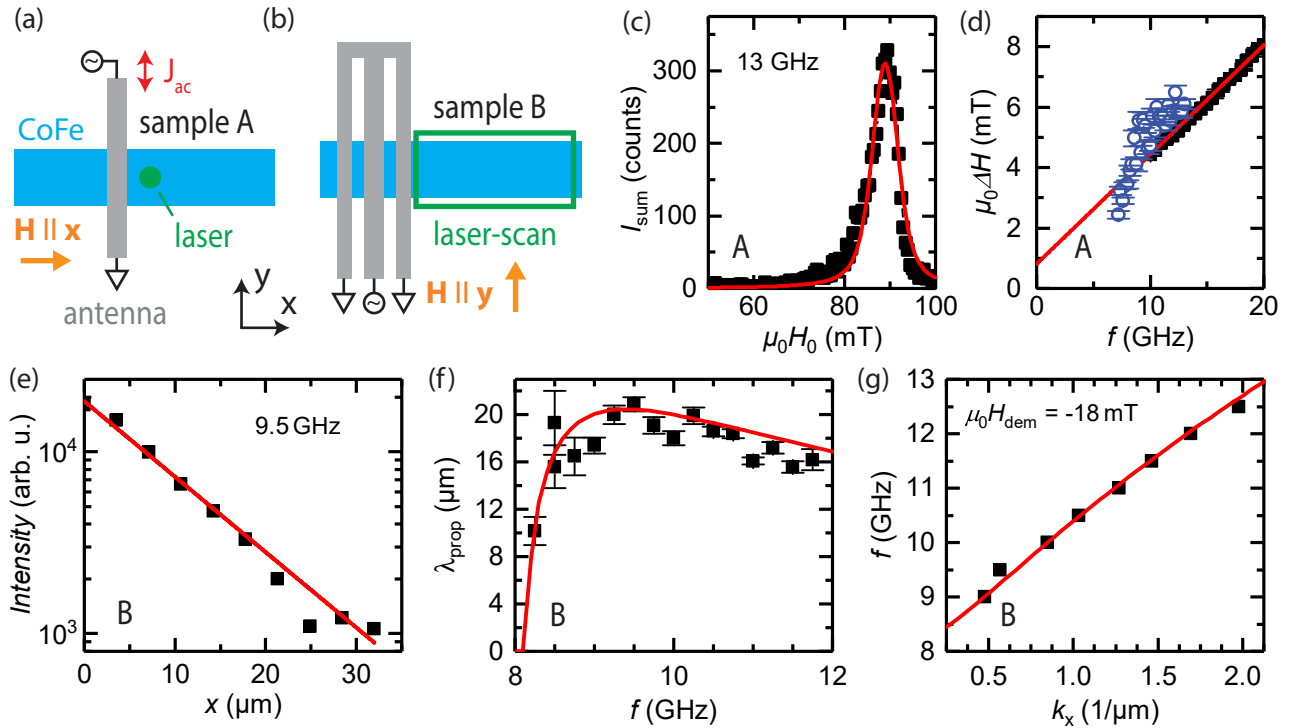


FIG. 3. (a), (b) Schematic depiction of sample A and B, respectively (top view). (c) Integrated BLS intensity vs. field. By use of a Lorentzian fit (red line), the linewidth is extracted and compared to values obtained by in-plane BB-FMR on a blanket film in (d). (e) Representative data set with  $f = 9.5$  GHz. The BLS intensity was measured as a function of the position  $(x, y)$  in the area highlighted with the green rectangle in (b). The measured signal was then integrated in  $y$  direction and the exponential decay in  $x$  direction is fitted (red curve). (f) Propagation length  $\lambda_{\text{prop}}$  for varying frequency  $f$ . Depicted error bars are fit errors. The red curve is based on an analytical model calculation (see text). (g) Experimentally determined  $f$  vs.  $k_x$  dispersion. The red line is a model from Eq. (8).

$k = \sqrt{k_x^2 + k_y^2}$  is the in-plane wave vector of the traveling spin wave. The calculation of the transversal wave vector component  $k_y = 0.31 \mu\text{m}^{-1}$  due to geometrical confinement was shown to be non-trivial and is used as a fitting parameter, as in Ref. 39. The resonances linewidth is given by<sup>40</sup>  $\Delta\omega = \alpha_{\text{eff}}\mu_0\gamma(M_{\text{eff}}/2 + H_0 + H_d)$  and the lifetime of the spin wave is  $\tau = 1/\Delta\omega$ . Here,  $\alpha_{\text{eff}} = \alpha_G - \alpha_{\text{rad}} + \gamma\mu_0 H_{\text{inh}}/(4\pi f_{\text{res}})$ <sup>41</sup>, where  $f_{\text{res}}$  is the resonance frequency. The propagation length is  $\lambda_{\text{prop}} = v_g\tau$ . The demagnetization field was set to  $\mu_0 H_d = -18$  mT, as required for matching Eq. (8) to the experimentally recorded dispersion shown in Fig. 3(g). Furthermore,  $\mu_0 M_{\text{eff}} = 2.36$  T and  $\mu_0 H_k = -70$  mT are obtained from Fig. 2(a). We find excellent agreement between this model and our experimental data in Fig. 3(f).

In summary, our sputter-deposited  $\text{Co}_{25}\text{Fe}_{75}$  layers exhibit a record low intrinsic damping for metallic ferromagnets of  $\alpha_0 = (1.45 \pm 1.60) \times 10^{-4}$ . The damping properties of extended films are maintained for micropatterned films, and spin-wave propagation lengths are in very good agreement with the properties extracted from BB-FMR. The low magnetic damping, together with the high saturation magnetization, lead to spin-wave decay lengths of more than  $20 \mu\text{m}$  at room temperature, which

are the highest reported so far in itinerant magnetic systems. This property makes  $\text{Co}_{25}\text{Fe}_{75}$  a promising material for all-metal spintronic and magnonic devices, compatible with semiconductor technology.

## ACKNOWLEDGMENTS

We acknowledge financial support by the Deutsche Forschungsgemeinschaft (DFG, German Research Foundation) via WE5386/4, WE5386/5 and Germany's Excellence Strategy EXC-2111-390814868.

- <sup>1</sup>P. Gambardella and I. M. Miron, Philosophical Transactions of the Royal Society A: Mathematical, Physical and Engineering Sciences **369**, 3175 (2011).
- <sup>2</sup>P. Wessels, A. Vogel, J. N. Tödt, M. Wieland, G. Meier, and M. Drescher, Scientific Reports **6**, 1 (2016).
- <sup>3</sup>A. Talalaevskij, M. Decker, J. Stigloher, A. Mitra, H. S. Körner, O. Cespedes, C. H. Back, and B. J. Hickey, Physical Review B **95**, 1 (2017).
- <sup>4</sup>H. S. Körner, M. A. W. Schoen, T. Mayer, M. M. Decker, J. Stigloher, T. Weindler, T. N. G. Meier, M. Kronseider, and C. H. Back, Applied Physics Letters **111**, 132406 (2017).
- <sup>5</sup>M. Collet, O. Gladii, M. Evelt, V. Bessonov, L. Soumah, P. Bortolotti, S. O. Demokritov, Y. Henry, V. Cros, M. Bailleul, V. E.

- Demidov, and A. Anane, *Applied Physics Letters* **110**, 092408 (2017).
- <sup>6</sup>I. S. Maksymov and M. Kostylev, *Physica E: Low-Dimensional Systems and Nanostructures* **69**, 253 (2015).
- <sup>7</sup>D. J. Twisselmann and R. D. McMichael, *Journal of Applied Physics* **93**, 6903 (2003).
- <sup>8</sup>V. E. Demidov, S. Urazhdin, A. Zholid, A. V. Sadovnikov, and S. O. Demokritov, *Applied Physics Letters* **105**, 172410 (2014).
- <sup>9</sup>V. V. Kruglyak, S. O. Demokritov, and D. Grundler, *Journal of Physics D: Applied Physics* **43**, 264001 (2010).
- <sup>10</sup>A. V. Chumak, V. I. Vasyuchka, A. A. Serga, and B. Hillebrands, *Nature Physics* **11**, 453 (2015).
- <sup>11</sup>C. Hauser, T. Richter, N. Homonnay, C. Eischmidt, M. Qaid, H. Deniz, D. Hesse, M. Sawicki, S. G. Ebbinghaus, and G. Schmidt, *Scientific Reports* **6**, 20827 (2016).
- <sup>12</sup>M. Evelt, V. E. Demidov, V. Bessonov, S. O. Demokritov, J. L. Prieto, M. Muñoz, J. Ben Youssef, V. V. Naletov, G. de Loubens, O. Klein, M. Collet, K. Garcia-Hernandez, P. Bortolotti, V. Cros, and A. Anane, *Applied Physics Letters* **108**, 172406 (2016).
- <sup>13</sup>M. B. Jungfleisch, W. Zhang, W. Jiang, H. Chang, J. Sklenar, S. M. Wu, J. E. Pearson, A. Bhattacharya, J. B. Ketterson, M. Wu, and A. Hoffmann, *Journal of Applied Physics* **117**, 17D128 (2015).
- <sup>14</sup>Houchen Chang, Peng Li, Wei Zhang, Tao Liu, A. Hoffmann, Longjiang Deng, and Mingzhong Wu, *IEEE Magnetics Letters* **5**, 1 (2014).
- <sup>15</sup>M. A. W. Schoen, J. M. Shaw, H. T. Nembach, M. Weiler, and T. J. Silva, *Physical Review B* **92**, 184417 (2015).
- <sup>16</sup>S. S. Kalarickal, P. Krivosik, M. Wu, C. E. Patton, M. L. Schneider, P. Kabos, T. J. Silva, and J. P. Nibarger, *Journal of Applied Physics* **99** (2006), 10.1063/1.2197087.
- <sup>17</sup>T. Sebastian, K. Schultheiss, B. Obry, B. Hillebrands, and H. Schultheiss, *Frontiers in Physics* **3**, 1 (2015).
- <sup>18</sup>Y. Sun, H. Chang, M. Kabatek, Y. Y. Song, Z. Wang, M. Jantz, W. Schneider, M. Wu, E. Montoya, B. Kardasz, B. Heinrich, S. G. Te Velthuis, H. Schultheiss, and A. Hoffmann, *Physical Review Letters* **111**, 1 (2013).
- <sup>19</sup>A. J. Berger, E. R. J. Edwards, H. T. Nembach, A. D. Karenowska, M. Weiler, and T. J. Silva, *Physical Review B* **97**, 094407 (2018).
- <sup>20</sup>C. Kittel, *Physical Review* **73**, 155 (1948).
- <sup>21</sup>G. Woltersdorf, F. Hoffmann, H. G. Bauer, and C. H. Back, *Physical Review B* **87**, 054422 (2013).
- <sup>22</sup>R. D. McMichael, D. J. Twisselmann, and A. Kunz, *Physical Review Letters* **90**, 4 (2003).
- <sup>23</sup>T. White, T. Bailey, M. Pierce, and C. W. Miller, *IEEE Magnetics Letters* **8**, 2015 (2017).
- <sup>24</sup>M. Haertinger, C. H. Back, J. Lotze, M. Weiler, S. Geprägs, H. Huebl, S. T. B. Goennenwein, and G. Woltersdorf, *Physical Review B* **92**, 054437 (2015).
- <sup>25</sup>Y. Tserkovnyak, A. Brataas, and G. E. W. Bauer, *Physical Review Letters* **88**, 117601 (2002).
- <sup>26</sup>S. J. Raeburn and R. V. Aldridge, *Journal of Physics F: Metal Physics* **8**, 1917 (1978).
- <sup>27</sup>J. W. De Vries, *Thin Solid Films* **167**, 25 (1988).
- <sup>28</sup>M. A. W. Schoen, D. Thonig, M. L. Schneider, T. J. Silva, H. T. Nembach, O. Eriksson, O. Karis, and J. M. Shaw, *Nature Physics* **12**, 839 (2016).
- <sup>29</sup>E. R. J. Edwards, H. T. Nembach, and J. M. Shaw, arXiv:1804.08786 (2018).
- <sup>30</sup>M. A. W. Schoen, H. T. Nembach, B. Koopmans, J. Lucassen, C. H. Back, T. J. Silva, and J. M. Shaw, *Physical Review B* **95**, 1 (2017).
- <sup>31</sup>J. M. Shaw, H. T. Nembach, T. J. Silva, and C. T. Boone, *Journal of Applied Physics* **114**, 243906 (2013).
- <sup>32</sup>B. Hillebrands and K. Ounadjela, *Spin Dynamics in Confined Magnetic Structures II*, edited by B. Hillebrands and K. Ounadjela, Topics in Applied Physics, Vol. 87 (Springer Berlin Heidelberg, Berlin, Heidelberg, 2003).
- <sup>33</sup>P. Pirro, T. Brächer, K. Vogt, B. Obry, H. Schultheiss, B. Leven, and B. Hillebrands, *Physica Status Solidi (B) Basic Research* **248**, 2404 (2011).
- <sup>34</sup>V. E. Demidov, M. P. Kostylev, K. Rott, P. Krzysteczko, G. Reiss, and S. O. Demokritov, *Applied Physics Letters* **95**, 112509 (2009).
- <sup>35</sup>P. Clausen, K. Vogt, H. Schultheiss, S. Schäfer, B. Obry, G. Wolf, P. Pirro, B. Leven, and B. Hillebrands, *Applied Physics Letters* **99**, 162505 (2011).
- <sup>36</sup>V. E. Demidov, S. Urazhdin, R. Liu, B. Divinskiy, A. Telegin, and S. O. Demokritov, *Nature Communications* **7**, 10446 (2016).
- <sup>37</sup>R. Matsumoto, A. Chanthbouala, J. Grollier, K. Yamanoi, S. Yakata, T. Kimura, and T. M. Á, **52**, 1 (2013).
- <sup>38</sup>B. A. Kalinikos and A. N. Slavin, *Journal of Physics C: Solid State Physics* **19**, 7013 (1986).
- <sup>39</sup>Z. Duan, I. N. Krivorotov, R. E. Arias, N. Reckers, S. Stienen, and J. Lindner, *Physical Review B* **92**, 104424 (2015).
- <sup>40</sup>D. D. Stancil and A. Prabhakar, *Spin Waves* (Springer, Boston, Ma, 2009) p. 332.
- <sup>41</sup>T. Wimmer, M. Althammer, L. Liensberger, N. Vlietstra, S. Geprägs, M. Weiler, R. Gross, and H. Huebl, arXiv:1812.01334 (2018).